Quaternary Science Reviews 143 (2016) 1–12

Contents lists available at ScienceDirect

Quaternary Science Reviews

journal homepage: www.elsevier.com/locate/quascirev

Precisely dated multidecadally resolved Asian summer monsoon dynamics 113.5–86.6 thousand years ago

Xiuyang Jiang [a, b, *], Xiaoyan Wang [a], Yaoqi He [c], Hsun-Ming Hu [d], Zhizhong Li [a, b], Christoph Spötl [e], Chuan-Chou Shen [d, **]

[a] Key Laboratory of Humid Subtropical Eco-geographical Processes, Ministry of Education, College of Geography Science, Fujian Normal University, Fuzhou 350007, China
[b] Institute of Geography, Fujian Normal University, Fuzhou 350007, China
[c] College of Tourism and Air Service, Guizhou Minzu University, Guiyang 550025, China
[d] High-Precision Mass Spectrometry and Environment Change Laboratory (HISPEC), Department of Geosciences, National Taiwan University, Taipei 106, Taiwan, ROC
[e] Institut für Geologie, Leopold-Franzens-Universität Innsbruck, Innrain 52, 6020 Innsbruck, Austria

ARTICLE INFO

Article history:
Received 26 July 2015
Received in revised form
24 April 2016
Accepted 7 May 2016

Keywords:
Asian summer monsoon
Sanxing Cave
MIS 5
Chinese interstadials
Precursor event

ABSTRACT

We present a new ^{230}Th-dated absolute chronology of Asian summer monsoon (ASM) variability from 113.5 to 86.6 kyr BP (before 1950 AD). This integrated multidecadally resolved record, based on 1435 oxygen isotope data and 46 ^{230}Th dates with 2-sigma errors as low as ±0.3 kyr from three stalagmites collected in Sanxing Cave, southwestern China, can be a new reference for calibrating paleoclimate proxy sequences. The Sanxing δ^{18}O record follows the 23 kyr precessional cycle of insolation and is punctuated by prominent millennial-scale oscillations of the Chinese Interstadials (CIS) 25 to 22, corresponding to Greenland Interstadials (GIS) 25 to 22. The onset of CIS 25, 24, 23 and 22 is dated to 113.1 ± 0.4, 108.1 ± 0.3, 103.7 ± 0.3 and 91.4 ± 0.6 kyr BP in the Sanxing record, respectively. The end of CIS 24 and CIS 22 is constrained to 105.5 ± 0.4 and 87.7 ± 0.3 kyr BP, respectively. A centennial-scale precursor event at 104.1 ± 0.3 kyr BP preceding CIS 23 is clearly registered. These events in the Sanxing record are synchronous with those identified in stalagmites from the European Alps (NALPS), except for the onset of GIS 25 and the end of GIS 22, and differ by up to 2.3 kyr from the corresponding ones in Greenland ice core records. The high degree of similarity of the δ^{18}O records between Sanxing Cave and Greenland supports a Northern Hemisphere forcing of the ASM. The anti-phase relationship of δ^{18}O records between Sanxing stalagmites and Antarctic ice cores suggests an additional ASM linkage to the Southern Hemisphere.

1. Introduction

Millennial and sub-millennial climatic variability is a key element of glacial periods as prominently documented by ice-core records (e.g., Dansgaard et al., 1993; McManus et al., 1999; North Greenland Ice Core Project Members, 2004; Capron et al., 2010a). These abrupt and recurrent variations, known as Dansgaard-Oeschger oscillations, were first described and numbered in Greenland ice cores (Dansgaard et al., 1993), with relatively warm Greenland interstadials (GIS) and cold Greenland stadials (GS) (Rousseau et al., 2006). Polar ice cores synchronized by methane (Blunier et al., 1998, 2007; Blunier and Brook, 2001) allowed to decipher the interhemispheric dynamics (Stocker and Johnsen, 2003). A milestone in the understanding of the precise linkage between high- and low-latitude climate variability was the study of Hulu Cave stalagmites (Wang et al., 2001), which demonstrated a tight correlation between the intensity of the Asian summer monsoon (ASM) and the North Atlantic climate during Marine Isotope Stages (MIS) 4-2, i.e. from 71 to 14 thousand years before present (kyr BP) (before AD 1950; note that all subsequent dates reported and discussed in the present study refer to this datum). This and subsequent speleothem records from this region provide a precisely dated template against which ice-core and other records

* Corresponding author. College of Geography Science, Fujian Normal University, Fuzhou 350007, China.
** Corresponding author.
E-mail addresses: xyjiang@fjnu.edu.cn (X. Jiang), river@ntu.edu.tw (C.-C. Shen).

http://dx.doi.org/10.1016/j.quascirev.2016.05.003
0277-3791/

can be compared, and demonstrate a fast response of the Asian monsoon (AM) to the climate variability in Northern Hemisphere (NH) high latitudes on decadal to millennial timescales (e.g. Wang et al., 2001, 2005; Gupta et al., 2003; Yuan et al., 2004; Liu et al., 2010; Deplazes et al., 2014; Zhao et al., 2010; Duan et al., 2014; Zhang et al., 2014). However, the sub-millennial to millennial-scale climate variability prior to MIS 4 is only poorly resolved by currently available speleothem records showing low-resolution and/or relatively large dating uncertainties (Kelly et al., 2006; Wang et al., 2008; Zhou et al., 2008; Li et al., 2014).

MIS 5 (130-70 kyr BP) (Shackleton, 1987), a period of relative small ice-sheet extent, large seasonal insolation changes, and high CO_2 concentrations, was characterized by remarkable long and low-frequency GIS events compared to MIS 3 (North Greenland Ice Core Project Members, 2004). However, our knowledge of the high-to-low latitudinal climate linkage during MIS 5 is limited by the scarcity of high-resolution AM records of sufficiently precise chronology. This difficulty has been exacerbated by several recent updates of ice-core age models (e.g., Wolff et al., 2010; Capron et al., 2010b; Veres et al., 2013).

A stalagmite record from central China suggests that the teleconnection between the ASM and high-latitude NH climate was significantly weaker between 120 and 110 kyr BP, i.e. during MIS 5d (Zhou et al., 2008). Zhou et al. (2008) proposed that the glacial boundary condition with low ice volume led to a decoupling of the ASM from the North Atlantic climate. Instead, stalagmite records from Dongge and Sanbao caves in southern and central China reveal a double ASM maximum during MIS 5c, corresponding to GIS 24 and 23 (Kelly et al., 2006; Wang et al., 2008), a period of lower ice volume than during MIS 5d (Lisiecki and Raymo, 2005). The NGRIP-EPICA Dronning Maud Land (EDML) common timescale shows a strong bipolar sequence of climate events during MIS 5 (Capron et al., 2010b). Additional prominent precursor events (PEs), also present in ice-core $\delta^{18}O$ and CH_4 records, preceded GIS 23 and 21 by 100–300 yr (Capron et al., 2010a). Absolutely dated records of comparable high resolution are a prerequisite to better understand the origin of monsoon variability on millennial and sub-millennial scales during times of reduced NH ice sheets.

Recent studies suggest differences between the ASM and NH high-latitude climate on orbital to sub-millennial scales. Additional forcing by the Southern Hemisphere (SH) via the cross-equatorial flow (Cai et al., 2006; Liu et al., 2008; An et al., 2011) or climatic feedbacks in the tropical Pacific (Partin et al., 2007) are thought to modulate the AM. Based on a comparison between Hulu Cave and ice-core records, Rohling et al. (2009), however, proposed a dominant control on millennial-scale monsoon variability by SH (NH) climate change during glacial (deglacial and interglacial) times when the monsoon is weak (strong). A detailed record of the AM during MIS 5, including the last glacial inception and the early stage of last glacial, is clearly needed to advance our understanding of the role of the NH versus the SH climates in influencing the ASM.

Here we present a new multidecadally resolved oxygen isotope record, covering the interval between 113.5 and 86.6 kyr BP, i.e. the early part of the last glacial period. The record is based on three stalagmites from Sanxing Cave, southwestern China, and is anchored by high-precision U–Th dates with uncertainties of less than 0.5%. The oxygen isotopes record the evolution of the ASM between Chinese interstadials (CIS) 25 and 22 in unprecedented detail. A comparison with NH and SH temperature records supports a teleconnection to the high-latitude climate. Furthermore, the MIS 5 portion of current ice-core timescales (Wolff et al., 2010; Capron et al., 2010b; Veres et al., 2013) is compared to this well-dated stalagmite record.

2. Site, material, and methods

Sanxing Cave (107°11′E, 27°22′N) is located in Tiechang, ~70 km southeast of Zuiyi City, Guizhou Province, southwestern China (Fig. S1). This 2 km-long cave, with only one entrance at an elevation of 720 m and a mean annual air temperature of 14.5 ± 0.5 °C, is located 270 km southeastward of Dongge Cave and 600 km northeastward of Sanbao Cave (Fig. 1). The regional climate is subtropical and characterized by distinct seasons, rainy hot summers and dry cold winters. Local mean annual air temperature, recorded at the nearest meteorological station (Zuiyi, 27°42′N, 106°52′E; elevation 844 m, 70 km NW of Sanxing Cave), is 13.5 ± 0.5 °C (1950-2000), ranges from 1.6 °C in winter to 22.5 °C in summer. Mean annual precipitation is 980 ± 50 mm (1 σ; 1950-2000) (Fig. S2). The cave is overlain by approximately 30 m of Permian limestone with a thin soil cover. The well-developed vegetation above the cave is dominated by subtropical broadleaf evergreen and a deciduous mixed forest.

Three calcitic stalagmites, SX7, SX24 and SX29, were collected in June 2012, approximately 900 m from cave entrance. They are 995, 358 and 420 mm long and 80, 70, and 65 mm in diameter, respectively (Fig. S3). For U–Th dating, 46 powdered subsamples (Fig. S3), ~50 mg each, were drilled from the polished cut surfaces of the stalagmites on a class-100 clean bench in a class-10,000 clean room. The procedure for chemical separation and purification of U and Th is described in Shen et al. (2002). An isotope dilution method with a ^{229}Th–^{233}U–^{236}U triple-spike tracer, calibrated with U–Th standards (Cheng et al., 2013) and isotopic equilibrium carbonate (Meyer et al., 2009), was employed (Shen et al., 2012). U–Th isotopic compositions and contents were determined using a Thermo-Fisher NEPTUNE multi-collection inductively coupled plasma mass spectrometer (MC-ICP-MS) at the High-Precision Mass Spectrometry and Environment Change Laboratory (HISPEC), Department of Geosciences, National Taiwan University (Shen et al., 2012). Uncertainties of ^{230}Th dates, relative to AD 1950, are calculated at the 2 σ level unless otherwise noted.

Powdered subsamples, 50–100 μg each, were obtained for $\delta^{18}O$ measurements using carbide dental burrs, 0.5 mm in diameter, by milling along the central growth axis at 1 or 2 mm intervals. A total number of 1435 subsamples were analyzed on a Finnigan MAT 253 mass spectrometer connected to an on-line, automated carbonate preparation system (Gasbench II) at the College of Geography Science, Fujian Normal University. Results are reported relative to Vienna Pee Dee Belemnite (VPDB) and standardization was accomplished using NBS-19. One-sigma reproducibility was ±0.06‰.

3. Results

3.1. U–Th dating

U–Th isotopic compositions and ^{230}Th dates are listed in Table 1. High ^{238}U concentrations ([^{238}U]) of 2–5 ppm and relatively low [^{232}Th] of 100–1000 ppt in SX7 and SX29 result in ^{230}Th dates with precisions mostly better than ±0.5% (Table 1). The difference between corrected and uncorrected ages is less than a few tens of years, which is 5–10 times less than the age uncertainty of ±100 s yrs. This indicates that initial detrital ^{230}Th is negligible. For stalagmite SX24, [^{238}U] is 384–860 ppb and [^{232}Th] 96–2080 ppt. The precision of the corrected ^{230}Th dates is ±301–502 yr. All ^{230}Th ages are in stratigraphic order. The chronology for each stalagmite was established using linear interpolation between individual ^{230}Th dates. The averaged temporal resolution of the oxygen isotope data is 32 yr for SX7, 31 yr for SX24, and 13 yr for SX29.

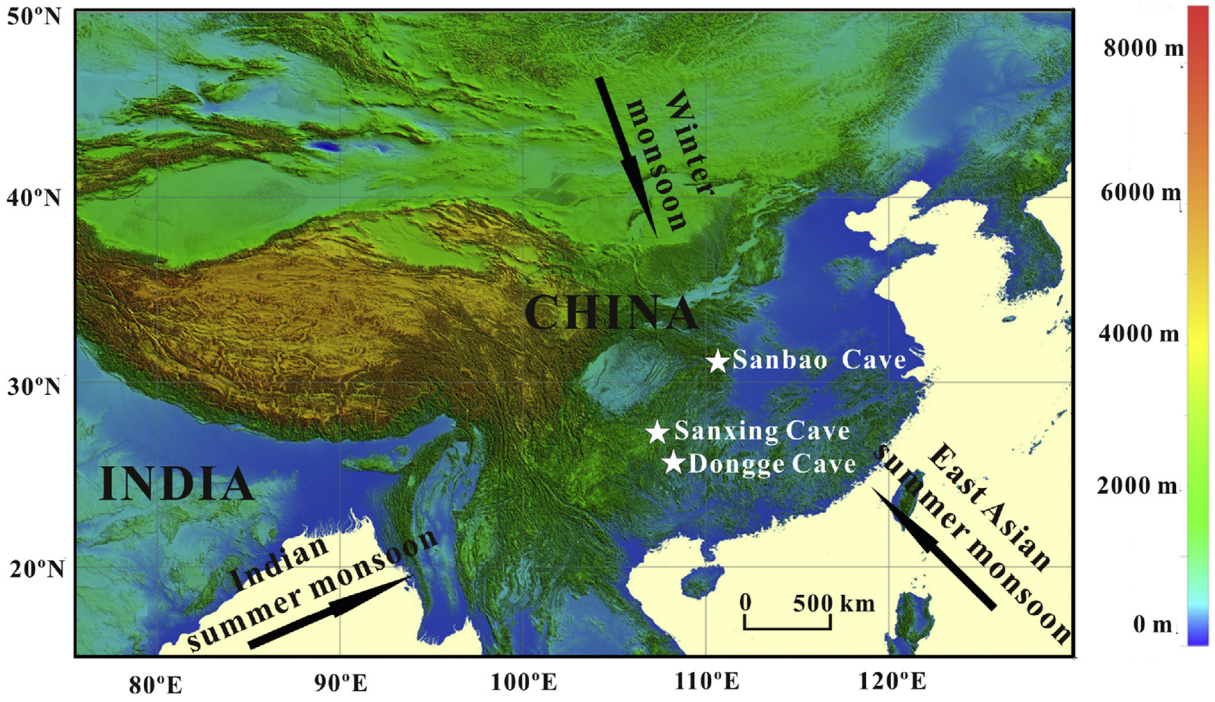

Fig. 1. Location of cave sites discussed in this paper: Sanbao Cave (Wang et al., 2005); Dongge Cave (Kelly et al., 2006) and Sanxing Cave (this study). Black arrows denote the directions of the East Asian summer monsoon, Indian summer monsoon, and East Asian winter monsoon, which affect the climate in China. This elevation map was generated using the software of Global Mapper 14.

3.2. Oxygen isotope records

Three methods were used to assess isotopic equilibrium vs. disequilibrium conditions during speleothem formation. Firstly, we compared the $\delta^{18}O$ and $\delta^{13}C$ values along the growth axis of each stalagmite and found no significant correlation ($r^2 = 0.02$ for SX7, 0.23 for SX24 and 0.0006 for SX29) (Fig. S4). Secondly, we measured the stable isotopic composition along six growth layers of three stalagmites (SX7, SX24 and SX29). The 2 σ variability of ±0.06–0.08‰ for the coeval $\delta^{18}O$ data (Fig. 2a) and the insignificant correlation ($0.01 < r^2 < 0.27$) between $\delta^{18}O$ and $\delta^{13}C$ values (Fig. 2b) suggest that the oxygen data pass the Hendy test (Hendy, 1971). Thirdly, there is no significant difference between the contemporaneous $\delta^{18}O$ records of stalagmites SX7 and SX24 during the interval 103.8–92.7 kyr BP and of stalagmites SX7 and SX29 for 108.3–106.2 kyr BP (Fig. 3), hence these speleothems also pass the replication test (Dorale and Liu, 2009). Calcite precipitation therefore occurred under conditions at an oxygen isotopic equilibrium and the speleothem data dominantly reflect the $\delta^{18}O$ value of meteoric precipitation and hence climate.

Previous studies from southern China showed that changes in stalagmite $\delta^{18}O$ values mainly record variations in summer monsoon intensity (e.g. Wang et al., 2005; Yuan et al., 2004; Cheng et al., 2009; Liu et al., 2010; Zhao et al., 2010). However, some observations and model simulations suggest that Chinese cave stalagmite $\delta^{18}O$ variations also reflect changes in moisture source(s) and/or water vapor pathways (Maher, 2008; Dayem et al., 2010; Pausata et al., 2011; Tan, 2014; Liu et al., 2015; Baker et al., 2015). In 2012, Cheng et al. clarified that the stalagmite $\delta^{18}O$-inferred ASM variations reflect a mean state of summer monsoon intensity or integrated moisture transport rather than the amount of local precipitation (Cheng et al., 2012). This is supported by a recent model simulation (Liu et al., 2014) and stalagmite multi-proxy records (Zhao et al., 2015; Duan et al., 2015) which confirm that the Chinese cave $\delta^{18}O$ records capture the monsoonal hydroclimate variability.

The isotopic composition of precipitation from the weather station Zuiyi shows a distinct monsoon-related seasonal variation (Fig. S2). Over 50% of the local annual precipitation occurs between June and August and only 6% between December and February. Modern rainfall data show that summer $\delta^{18}O$ values are over 6‰ lower than winter values (−9.7 vs. −3.3‰; Fig. S2). On the basis of instrumental data and previous studies, we interpret the Sanxing calcite $\delta^{18}O$ values as changes in the variability of monsoonal rainfall amount, combined with changes in moisture trajectory and seasonal distribution of rainfall.

The $\delta^{18}O$ values of three stalagmites change dramatically throughout the whole record and range from −9.3 to −5.2‰, with maximum values at 96.0–92.1 kyr BP (Fig. 3). The largest $\delta^{18}O$ excursion with a magnitude of 3.2‰ occurred between 100.0 and 96.0 kyr BP, indicating a major climatic shift between MIS 5c and 5b (Fig. 3). Three distinct features are expressed in the replicated Sanxing $\delta^{18}O$ record spanning from 113.5 to 86.6 kyr BP (Figs. 3, 4c): (1) the record tracks NH summer insolation, (2) four significant increases by 0.5–1.5‰ are superimposed on this orbitally forced trend indicating high summer monsoon intensity (CIS 25-22; Wang et al., 2008), and (3) a centennial-scale strong summer monsoon event preceded CIS 23.

4. Discussion

4.1. Coherence and timing of monsoon events

The new Sanxing stalagmite $\delta^{18}O$ sequence shows a strong ASM during MIS 5c and two weak ASM intervals during MIS 5d and 5b (Fig. 3). They are aligned with events recorded in other Chinese caves, such as Sanbao (Wang et al., 2008; Cheng et al., 2009) and Dongge cave (Kelly et al., 2006) (Fig. 4). This synchroneity of

Table 1
U–Th dating results for stalagmites SX7, SX24 and SX29, from Sanxing Cave.

Sample number	Depth (cm)	^{238}U (ng/g)	^{232}Th (pg/g)	δ^{234}U (measured)	^{230}Th/^{238}U (activity)	^{230}Th age (kyr) (uncorrected)	^{230}Th age (kyr BP) (corrected)	$\delta^{234}U_{inital}$ (corrected)
SX7-10	1.0	2787 ± 4	2218 ± 13	1333 ± 4	1.362 ± 0.004	86.7 ± 0.4	**86.6 ± 0.4**	1703 ± 6
SX7-30	3.0	2898 ± 4	232 ± 8	1271 ± 4	1.338 ± 0.003	88.0 ± 0.3	**87.9 ± 0.3**	1630 ± 5
SX7-60	6.0	2099 ± 2	490 ± 10	1276 ± 3	1.355 ± 0.002	89.2 ± 0.3	**89.1 ± 0.3**	1642 ± 4
SX7-110	11.0	1696 ± 1	454 ± 11	1261 ± 3	1.361 ± 0.003	90.7 ± 0.3	**90.6 ± 0.3**	1629 ± 4
SX-7-143	14.3	2755 ± 5	210 ± 9	1273 ± 4	1.378 ± 0.006	91.5 ± 0.6	**91.4 ± 0.6**	1649 ± 6
SX7-232	23.2	4145 ± 5	83 ± 10	1216 ± 3	1.350 ± 0.002	92.4 ± 0.3	**92.3 ± 0.3**	1579 ± 4
SX-7-330	33.0	879 ± 1	552 ± 9	1490 ± 4	1.559 ± 0.005	95.3 ± 0.5	**95.2 ± 0.5**	1949 ± 6
SX7-380	38.0	1981 ± 2	174 ± 10	1350 ± 3	1.475 ± 0.002	96.1 ± 0.3	**96.0 ± 0.3**	1771 ± 4
SX7-420	42.0	1157 ± 1	87 ± 10	1405 ± 3	1.516 ± 0.003	96.5 ± 0.3	**96.4 ± 0.3**	1845 ± 4
SX7-452	45.2	869 ± 1	130 ± 11	1424 ± 3	1.534 ± 0.002	97.1 ± 0.3	**97.0 ± 0.3**	1873 ± 4
SX7-500	50.0	814 ± 1	126 ± 10	1462 ± 3	1.567 ± 0.002	97.7 ± 0.3	**97.7 ± 0.3**	1928 ± 4
SX7-512	51.2	1752 ± 3	177 ± 8	1271 ± 4	1.456 ± 0.003	99.4 ± 0.4	**99.3 ± 0.4**	1683 ± 5
SX7-528	52.8	2894 ± 4	331 ± 8	1236 ± 3	1.444 ± 0.003	100.5 ± 0.4	**100.5 ± 0.4**	1643 ± 5
SX7-550	55.0	2530 ± 3	65 ± 13	1231 ± 3	1.445 ± 0.002	101.0 ± 0.3	**100.9 ± 0.3**	1638 ± 4
SX7-628	62.8	2978 ± 2	239 ± 11	1186 ± 3	1.425 ± 0.002	102.2 ± 0.3	**102.1 ± 0.3**	1582 ± 4
SX7-662	66.2	4636 ± 5	135 ± 10	1164 ± 3	1.414 ± 0.003	102.7 ± 0.4	**102.6 ± 0.4**	1555 ± 4
SX7-680	68.0	3765 ± 4	180 ± 9	1171 ± 3	1.421 ± 0.002	102.9 ± 0.3	**102.9 ± 0.3**	1566 ± 4
SX7-724	72.4	6051 ± 8	185 ± 8	1108 ± 3	1.386 ± 0.003	103.9 ± 0.4	**103.9 ± 0.4**	1486 ± 5
SX7-744	74.4	3469 ± 4	169 ± 10	1106 ± 3	1.386 ± 0.002	104.1 ± 0.3	**104.0 ± 0.3**	1484 ± 4
SX7-764	76.4	6945 ± 9	226 ± 8	1076 ± 3	1.374 ± 0.003	105.0 ± 0.4	**105.0 ± 0.4**	1448 ± 4
SX7-782	78.2	7711 ± 9	279 ± 9	1094 ± 3	1.387 ± 0.002	105.1 ± 0.4	**105.0 ± 0.4**	1472 ± 4
SX7-810	81.0	3995 ± 6	585 ± 13	1125 ± 3	1.413 ± 0.003	105.5 ± 0.4	**105.5 ± 0.4**	1516 ± 5
SX7-856	85.6	3189 ± 3	359 ± 11	1155 ± 3	1.437 ± 0.002	105.9 ± 0.3	**105.8 ± 0.3**	1558 ± 4
SX7-890	89.0	4028 ± 5	620 ± 8	1167 ± 3	1.452 ± 0.003	106.6 ± 0.4	**106.6 ± 0.4**	1577 ± 5
SX7-914	91.4	5444 ± 8	476 ± 9	1108 ± 4	1.417 ± 0.003	107.5 ± 0.5	**107.4 ± 0.5**	1501 ± 5
SX7-932	93.2	5886 ± 7	160 ± 11	1088 ± 3	1.406 ± 0.002	107.8 ± 0.4	**107.7 ± 0.4**	1475 ± 4
SX7-960	96.0	4719 ± 7	479 ± 8	1174 ± 4	1.471 ± 0.004	108.1 ± 0.6	**108.1 ± 0.6**	1593 ± 6
SX7-976	97.6	3837 ± 6	675 ± 9	1190 ± 4	1.484 ± 0.004	108.3 ± 0.6	**108.2 ± 0.6**	1615 ± 6
SX24-5	0.5	653 ± 1	1380 ± 9	1779 ± 6	1.717 ± 0.005	92.9 ± 0.5	**92.8 ± 0.5**	2313 ± 9
SX24-55	5.5	576 ± 1	2080 ± 7	1746 ± 3	1.719 ± 0.006	94.6 ± 0.5	**94.5 ± 0.5**	2280 ± 5
SX24-170	17.0	402 ± 0	261 ± 4	1594 ± 4	1.652 ± 0.004	97.4 ± 0.4	**97.3 ± 0.4**	2098 ± 5
SX24-182	18.2	418 ± 0	1479 ± 8	1574 ± 4	1.651 ± 0.004	98.4 ± 0.4	**98.3 ± 0.4**	2077 ± 6
SX24-225	22.5	384 ± 0	150 ± 5	1515 ± 3	1.614 ± 0.004	98.7 ± 0.4	**98.6 ± 0.4**	2001 ± 5
SX24-240	24.0	513 ± 1	250 ± 7	1536 ± 4	1.637 ± 0.004	99.5 ± 0.4	**99.4 ± 0.4**	2033 ± 6
SX24-269	26.9	503 ± 0	96 ± 6	1537 ± 2	1.643 ± 0.003	99.9 ± 0.3	**99.8 ± 0.3**	2038 ± 4
SX24-280	28.0	453 ± 1	477 ± 5	1547 ± 3	1.659 ± 0.004	100.7 ± 0.4	**100.7 ± 0.4**	2055 ± 5
SX24-355	35.5	860 ± 1	142 ± 5	1498 ± 3	1.658 ± 0.003	103.8 ± 0.3	**103.7 ± 0.3**	2008 ± 4
SX29-30	3.0	3799 ± 4	914 ± 8	1093 ± 3	1.400 ± 0.003	106.3 ± 0.4	**106.3 ± 0.4**	1476 ± 4
SX29-80	8.0	1768 ± 1	255 ± 8	1178 ± 2	1.465 ± 0.002	107.3 ± 0.3	**107.2 ± 0.3**	1595 ± 3
SX29-125	12.5	2760 ± 2	204 ± 7	1159 ± 2	1.458 ± 0.002	108.0 ± 0.3	**107.9 ± 0.3**	1572 ± 3
SX29-172	17.2	2335 ± 1	169 ± 8	1129 ± 2	1.439 ± 0.002	108.3 ± 0.3	**108.2 ± 0.3**	1533 ± 3
SX29-185	18.5	1999 ± 1	611 ± 9	1334 ± 2	1.591 ± 0.003	108.7 ± 0.3	**108.7 ± 0.3**	1814 ± 3
SX29-235	23.5	2881 ± 2	320 ± 8	1392 ± 2	1.638 ± 0.003	109.3 ± 0.3	**109.2 ± 0.3**	1896 ± 3
SX29-245	24.5	3688 ± 3	109 ± 7	1168 ± 2	1.494 ± 0.002	111.3 ± 0.3	**111.3 ± 0.3**	1600 ± 3
SX29-265	26.5	2931 ± 4	371 ± 6	1227 ± 3	1.546 ± 0.002	112.2 ± 0.4	**112.2 ± 0.4**	1685 ± 4
SX29-415	41.5	4142 ± 3	293 ± 8	1142 ± 2	1.493 ± 0.002	113.5 ± 0.3	**113.5 ± 0.3**	1574 ± 3

Uncertainties are 2 σ analytical errors. Decay constant values are $\lambda_{230} = 9.1705 \times 10^{-6}\ yr^{-1}$, $\lambda_{234} = 2.82206 \times 10^{-6}\ yr^{-1}$, $\lambda_{238} = 1.55125 \times 10^{-10}\ yr^{-1}$. Corrected ^{230}Th ages (kyr BP, before 1950 AD) are calculated using an estimated initial ^{230}Th/^{232}Th atomic ratio of $4 \pm 2 \times 10^{-6}$ and indicated in bold.

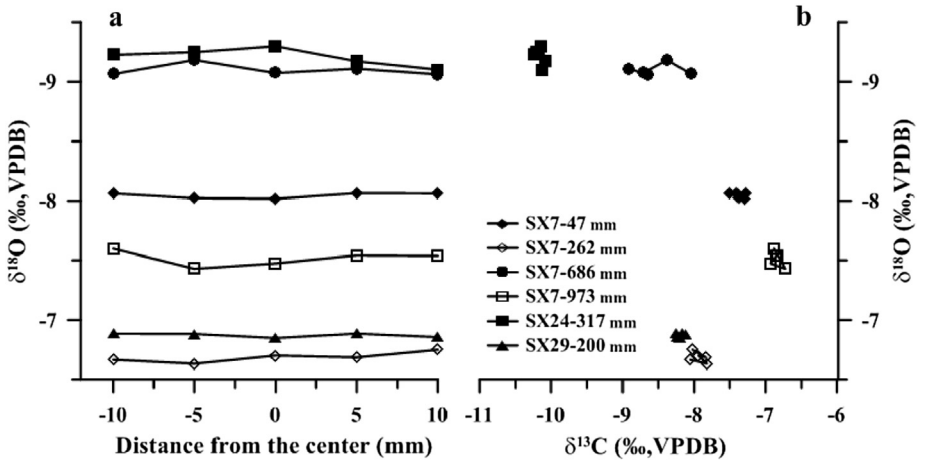

Fig. 2. Hendy tests along six growth layers of three stalagmites. **(a)** One-sigma δ^{18}O variability within growth layers varies by ±0.06–0.08‰. **(b)** Plots of δ^{18}O versus δ^{13}C for coeval subsamples.

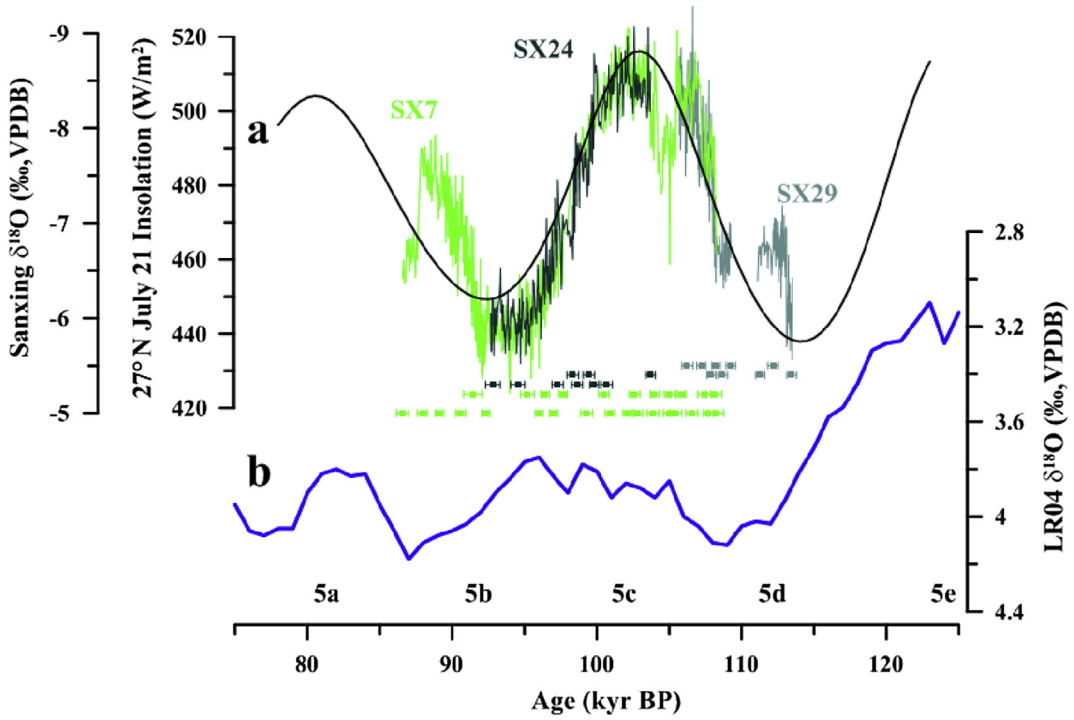

Fig. 3. Comparison of **(a)** $\delta^{18}O$ time series of stalagmites SX7 (green), SX24 (dark green), and SX29 (ocean green) with insolation (black) (Berger and Loutre, 1991) and **(b)** benthic foraminiferal $\delta^{18}O$-inferred ice volume (blue) (Lisiecki and Raymo, 2005). ^{230}Th ages and errors are color-coded by stalagmite. MIS substages are listed at the bottom. (For interpretation of the references to colour in this figure legend, the reader is referred to the web version of this article.)

stalagmite $\delta^{18}O$ dynamics between different regions in mainland China indicates that the ASM intensity primarily follows NH summer insolation (NHSI) on orbital timescales and is driven by precessional forcing (e.g., Wang et al., 2008; Cheng et al., 2009) (Fig. 4).

As illustrated in Fig. 4, multi-millennial to centennial-scale oscillations are also an important element of the Sanxing Cave profile. The record exhibits four strong millennial-scale summer monsoon events, CIS 25-22 (Wang et al., 2008) (Fig. 4). A rapid decrease in $\delta^{18}O$ by up to 0.7‰ at 113.1 ± 0.4 kyr BP suggests an abrupt resumption of summer monsoon intensity at the onset of CIS 25. The timing of this event is consistent with the Sanbao Cave record (Wang et al., 2008) within dating error (Fig. 4a, c), but not clearly expressed in the Dongge $\delta^{18}O$ record (Kelly et al., 2006) (Fig. 4b).

The multidecadally resolved Sanxing $\delta^{18}O$ record shows an abrupt onset of CIS 24 at the MIS 5d/5c transition (Figs. 3, 4c). Especially for the SX29 record, the chronology is tightly anchored by six ^{230}Th ages with a mean uncertainty of ±0.3 kyr. Two dates, 108.2 ± 0.3 and 107.9 ± 0.3 kyr BP at the beginning and end of the sharp onset of CIS 24, respectively, constrain the mid-point of the transition to 108.1 ± 0.3 kyr BP (Fig. S5). This timing agrees with the Sanbao and Dongge records which, however, lack dating points at this transition (Fig. 4).

The CIS 24 event is immediately followed by a weak monsoon event lasting from 105.5 to 104.2 kyr BP, with a sharp 1.5‰ positive excursion in $\delta^{18}O$ at 105.0 kyr BP. The timing of this event is consistent with the Sanbao and Dongge records within dating uncertainty, but the superimposed sharp excursion has not been documented in the Sanbao $\delta^{18}O$ records (Fig. 4). Interestingly, the Dongge $\delta^{18}O$ record shows two positive sub-centennial shifts at 105.4 and 105.2 kyr BP during this weak monsoon event (Fig. 4b), highlighting the need for further high-resolution studies.

The onset of CIS 23 is dated to 103.7 ± 0.3 kyr BP in the Sanxing record, consistent with the Sanbao and Dongge records, despite their larger errors of ±0.9 kyr. The mid-point of the transition into CIS 22 occurs at 91.4 ± 0.6 kyr BP in Sanxing Cave (Fig. S6), matching the one in Sanbao record within the dating uncertainty of ±0.8 kyr (Fig. 4a, c). The end of CIS 22 is dated to 87.7 ± 0.3 kyr BP in the Sanxing $\delta^{18}O$ record, identical with the Sanbao data (Fig. 4).

Overall, the Sanxing, Sanbao and Dongge records show consistent $\delta^{18}O$ profiles on orbital to millennial timescales, underscoring the regional significance of speleothem-based $\delta^{18}O$ records from southern China. This consistency reflects large-scale circulation and precipitation patterns associated with ASM dynamics. The Sanxing record is superior to the Sanbao and Dongge records in three aspects. Firstly, the chronology is anchored by 46 ^{230}Th dates with typical errors of only ±300–600 yrs, significantly reducing the uncertainty of the timing of rapid monsoon events. Secondly, the resolution of 100–450 yr during the time interval 116-86 kyr BP in the Sanbao record has been increased to 30 yrs in the new Sanxing record, allowing a detailed correlation of individual monsoon events to GIS 25-22. Lastly, a centennial-scale PE preceding CIS 23 is clearly documented in the Sanxing record at 104.2–103.9 kyr BP (Fig. 4c), providing an important chronological marker for other climate archives, such as ice cores and sediments.

4.2. Comparison of Sanxing and Greenland ice-core records and chronological implications

As illustrated in Fig. 5, four strong summer monsoon events (CIS 25-22) in the Sanxing record agree with the corresponding GIS events in Greenland. However, different ice-core timescales result in different offsets between the two records. This discrepancy is most likely attributed to the limited accuracy of the ice-core age models. The multi-parameter and annual layer-counted GICC05 timescale covers the past 60 kyr BP (Svensson et al., 2008), confirmed by ^{230}Th-dated speleothem chronologies (e.g. Wang et al., 2001; Genty et al., 2003; Cruz et al., 2005; Spötl et al., 2006). Wolff et al. (2010), however, stressed that large

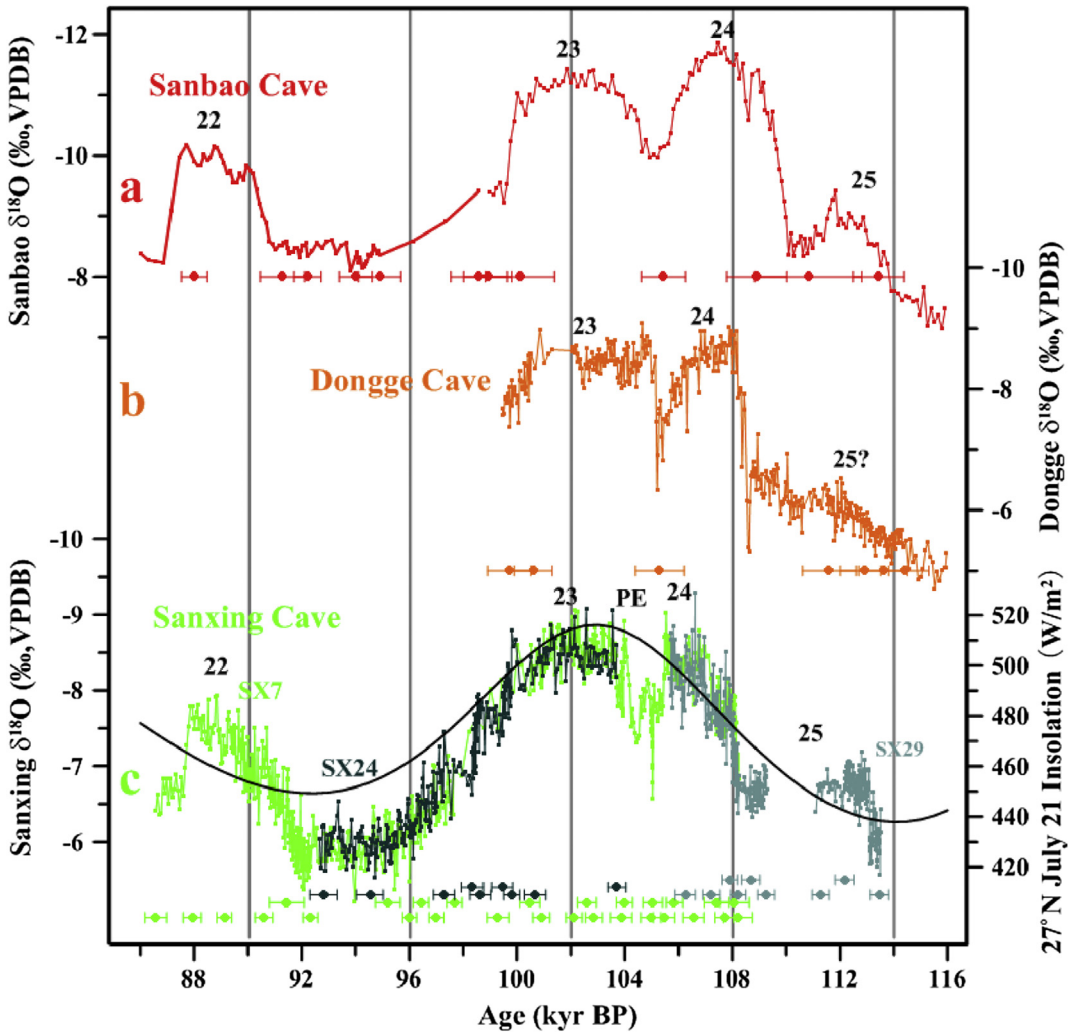

Fig. 4. Comparison of $\delta^{18}O$ records between Sanxing, Sanbao, and Dongge Caves. **(a)** Spliced stalagmite $\delta^{18}O$ record from Sanbao Cave (Wang et al., 2008). **(b)** Dongge $\delta^{18}O$ record (Kelly et al., 2006). **(c)** Sanxing $\delta^{18}O$ record (this study). ^{230}Th ages and errors are color-coded by cave. Numbers 22-25 mark millennial-scale humid events. PE donates a precursor event preceding GIS/CIS 23.

uncertainties still exist in the current Greenland ice-core age models for the first half of the last glacial period between 118 and 60 kyr BP.

Ice-core chronologies have been significantly refined over the past decades. The GICC05modelext timescale (Wolff et al., 2010) superseded the previous ss09sea timescale (North Greenland Ice Core Project Members, 2004) for the first half of the last glacial. On the basis of the synchronization between NGRIP and EDML by atmospheric $\delta^{18}O$ ($\delta^{18}O_{atm}$) and CH_4 measurements between 123 and 80 kyr BP, Capron et al. (2010b) presented the first continuous sequence of the north-south climatic dynamics on a common EDML-NGRIP ice timescale (transferring the NGRIP record onto the EDML1 timescale - Ruth et al., 2007; Capron et al., 2010a) (Fig. 5b), thereby reducing relative dating uncertainties. Recently, using an optimized multi-parameter and multi-site dating approach, Veres et al. (2013) presented a new Antarctic ice core age model (AICC 2012; Fig. 5c). Within the interval 116-100 kyr BP this chronology differs from EDML1 by a few hundred years and is younger than GICC05modelext by a couple of thousand years (Fig. 5). In 2011, Boch et al. (2011) presented an integrated ^{230}Th-dated stalagmite $\delta^{18}O$ record (Fig. 5e) from the northern rim of the Alps (NALPS) for the interval from 120 to 60 kyr BP, providing a promising reference for Greenland ice-core records. The tightly ^{230}Th-dated CIS events 25-22 in the Sanxing record between 113.5 and 86.6 kyr BP provide even more precise constraints to evaluate current ice-core timescales (Fig. 5d).

In Fig. 5 and Table 2, NGRIP $\delta^{18}O$ records on the GICC05modelext, EDML1, and AICC2012 timescales are compared with the Sanxing stalagmite $\delta^{18}O$ record for the interval 116 to 86 kyr BP. The rapid transition into GIS 25, the first GIS event in the last glacial, is constrained to 112.4 kyr BP and 112.6 kyr BP by the EDML1 and AICC2012 timescales, respectively, which is only 0.7 and 0.5 kyr, respectively, younger than the transition into CIS 25 at 113.1 ± 0.4 kyr BP in the Sanxing record. GICC05modelext model suggests a transition 2.3 kyr older than the stalagmite record (Fig. 5a and d). No significant age difference is found for the onset of GIS/CIS 24 and 23 and the end of GIS/CIS 24 between the Greenland ice-core record on the GICC05modelext timescale and the Sanxing record. On the DML1 and AICC2012 timescales, however, these transitions are 1.3–2.3 kyr younger in Greenland than in Sanxing. An offset of 1.4–1.9 kyr is observed for the onset of GIS 22 on all three timescales (Fig. 5). The abrupt termination of GIS 22 at 87.7 kyr BP on the GICC05modelext and EDML1 timescales matches its counterpart in the Sanxing record at 87.7 ± 0.3 kyr BP, but is

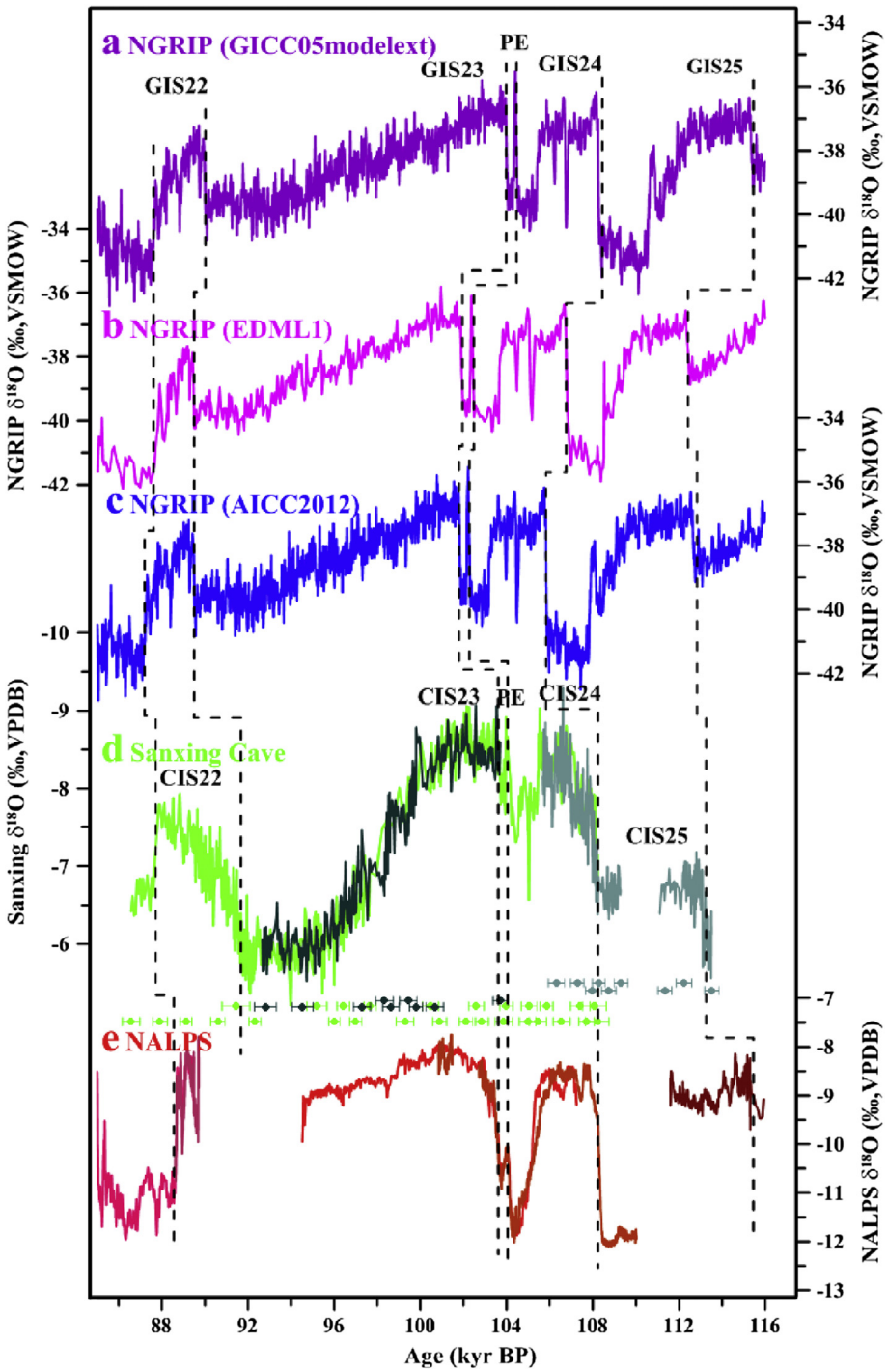

Fig. 5. Comparison of $\delta^{18}O$ records between Sanxing Cave, European Alpine caves (NALPS), and NGRIP ice core from 116 to 86 kyr BP. NGRIP record on timescales of **(a)** GICC05modelext (Wolff et al., 2010), **(b)** EDML1 (Capron et al., 2010b), and **(c)** AICC 2012 (Veres et al., 2013). **(d)** Sanxing $\delta^{18}O$ record (this study). **(e)** NALPS $\delta^{18}O$ record (Boch et al., 2011). ^{230}Th ages and errors are color-coded by stalagmite for Sanxing Cave. Gray dashed lines link mid-points of major GIS/CIS transitions and the PE at 104.1 kyr BP. GIS 22-25 and CIS 22-25 are the millennial-scale warm and humid events in Greenland and China, respectively.

~0.5 kyr younger on the AICC2012 timescale.

The events in the Sanxing record are synchronous within dating error with those in the NALPS record except for the onset of GIS 25 and the end of GIS 22 (Fig. 5, Table 2, Boch et al., 2011), known to share the same climate forcing as Greenland, but up to 2.3 kyr older than ones in NGRIP on the EDML1 and GICC2012 timescales (Table 2). Our Sanxing record is - within dating error - in good agreement with the NGRIP record on the GICC05modelext timescale (Wolff et al., 2010), except for the abrupt warmings of GIS 25 and GIS 22 (Fig. 5, Table 2). Our record together with NALPS provides tight chronological constraints on monsoon variability and European climate during MIS 5.

4.3. A precursor event preceding CIS 23

The NGRIP profile shows a 200-300 yr-long warming event

Table 2
Comparison of the timing of GIS/CIS 22-25 and the PE between the Sanxing stalagmite and ice-core age records on different timescales.

Event	Timing (kyr BP)									
	Sanxing	Error 2σ	NALPS	Error 2σ	NGRIP (GICC05modelext)	Difference to Sanxing	NGRIP (EDML1)	Difference to Sanxing	NGRIP (AICC 2012)	Difference to Sanxing
GIS 25 onset	113.1	±0.4	115.3	±0.5	115.4	+2.3	112.4	−0.7	112.6	−0.5
GIS 24 onset	108.1	±0.3	108.3	±0.5	108.3	+0.2	106.8	−1.3	105.8	−2.3
GIS 24 termination	105.5	±0.4	105.2	±0.5	105.4	−0.1	103.7	−1.8	103.2	−2.3
GIS 23 Precursor event	104.1	±0.3	104.0	±0.3	104.4	+0.3	102.4	−1.7	102.2	−1.9
GIS 23 onset	103.7	±0.3	103.6	±0.4	104.0	+0.3	101.9	−1.8	101.8	−1.9
GIS 22 onset	91.4	±0.6	Hiatus		90.0	−1.4	89.5	−1.9	89.5	−1.9
GIS 22 termination	87.7	±0.3	88.7	±0.3	87.7	0.0	87.7	0.0	87.2	−0.5

preceding GIS 23, referred to as PE (Capron et al., 2010a), which is recorded by a spike in methane concentration (Capron et al., 2010b) as well as in oxygen (Capron et al., 2010a) and nitrogen isotope data (Landais et al., 2006, Fig. 6). This event was also observed in a multi-annually resolved sediment record from Cariaco Basin on the northern shelf of Venezuela (Deplazes et al., 2013) and in the NALPS stalagmite record from the European Alps (Boch et al., 2011). This event is not clearly expressed in previous Chinese stalagmite records (Kelly et al., 2006; Wang et al., 2008; Cheng et al., 2009) due to their limited temporal resolution (Fig. 4a, b). The bi-decadally resolved Sanxing record clearly registers this PE as a strong ASM interval from 103.9 to 104.2 kyr BP (Fig. 6). Onset and termination occurred within <200 and 100 yr, respectively (Fig. 6). The first-time identification of this PE in Asia suggests a large-scale climatic footprint of the NH high latitudes on the ASM.

The PE prior to GIS 23 is centered at 104.4, 102.4 and 102.2 kyr BP in NGRIP on the GICC05modelext, EDML1 and AICC2012 timescales, respectively (Fig. 5; Table 2). The first ^{230}Th-dated duration of this event - in the NALPS stalagmite record - is between 104.2 and 103.8 kyr BP with an uncertainty of ±0.4 kyr (Boch et al., 2011) (Fig. 6). The Sanxing record shows that this event is centered at 104.1 ± 0.3 kyr BP and lasted about 300 years, constrained with two precise ^{230}Th dates, consistent with the NALPS record (Boch et al., 2011), but older than that in NGRIP records on the EDML1 and AICC2012 timescales by ~2 kyr, if dating errors are not considered (Fig. 5). There is no significant age difference between the Sanxing record and Greenland on the GICC05modelext timescale (Figs. 5 and 6; Table 2). This chronological marker is therefore an excellent candidate for calibrating Greenland ice-core records.

The striking similarity of sub-millennial-scale PE identified in Greenland and AM records is not only apparent during MIS 5, but also during early MIS 3 (Liu et al., 2010) and MIS 3/2 (Zhao et al., 2010). This linkage, a persistent feature of glacial periods, suggests that atmospheric circulation changes are important in transmitting abrupt climate signals from high to low latitudes (Liu et al., 2010; Zhao et al., 2010), e.g. via northward/southward shifts of the Intertropical Convergence Zone (ITCZ) (Deplazes et al., 2013). As the wind field is of primary importance in linking different climate systems (Mikolajewicz et al., 1997), a shift in Atlantic thermohaline circulation associated with changes in sea ice extent (Vidal et al., 1998) could provide a teleconnection with hydrological and thermal conditions in the low-latitudes (Stott et al., 2002).

4.4. Influence of NH and SH climates on the ASM

The millennial-to centennial-scale CIS 24-22 events recorded in the Sanxing record closely match the δ^{18}O record of Greenland ice cores, indicating that the link between NH high-latitude climate and the AM is a persistent element of the global climate (Wang et al., 2008). The millennial-to centennial-scale AM variability during MIS 5 may also result from interactions between northern high-latitude cold air advection and summer moisture transported across the tropical ocean (Sun et al., 2011; Deplazes et al., 2014). A coupling mechanism possibly exists between high-latitude temperature, tropical moisture transport, AM circulation, and the mean position of the ITCZ (Yancheva et al., 2007; Fleitmann et al., 2007; Wang et al., 2008; Sun et al., 2011; Deplazes et al., 2014).

Although the CIS 24-22 events agree with millennial-centennial climatic changes in the North Atlantic region, small-scale features differ. GIS 24-22 events started abruptly with an initial warming, followed by a gradual cooling over several millennia and a rapid temperature drop leading to following stadial (Capron et al., 2010b) (Fig. 7). The Sanxing record, however, exhibits significantly different trends. For CIS 24 and CIS 22, ASM intensity increased rapidly at the beginning, slowly approached a maximum during the following several thousands of years, and then suddenly decreased to Chinese stadials (CS) (Fig. 7). After its initial abrupt increase, the CIS 23 event shows an increasing trend in the first 2 kyr and then a decrease (Fig. 7). Similar features were also observed in other monsoon records of MIS 4-2 when large ice sheets existed in the NH. For example, Duan et al. (2014) and Deplazes et al. (2013) showed that the onset of GIS events during MIS 4-2 at low latitudes occurred in at least two steps. After an initial abrupt shift it took several decades to a few centuries for CIS events to reach the monsoonal maxima (Duan et al., 2014; Deplazes et al., 2013).

Previous studies suggested that the sawtooth structure of DO events in Greenland ice cores is related to changes in sea-ice coverage in the Nordic seas and regional changes in precipitation (e.g., Li et al., 2010). The decoupling between Greenland temperature and the ASM during interstadials suggests that this asymmetric temperature and precipitation pattern is not a perfect template for tropical hydroclimate change during the glacial. It implies that additional mechanism(s) modulate the evolution of the monsoon intensity and the low-latitude hydrological cycle.

The pattern of CIS 24-22 in the Sanxing record is broadly anti-phase with the EDML ice-core δ^{18}O record from Antarctica, with increasing (decreasing) monsoon intensity corresponding to lower (higher) Antarctic temperature (Fig. 7). Antarctic Isotope Maxima (AIM) events are marked by a gradual warming during the GS, followed by a gradual cooling over several millennia during the GIS, like a "∧" pattern (EPICA Community Members, 2006). Antarctic climate imprints have been reported in records from the tropics (Altabet et al., 2002), subtropics (Cai et al., 2006), temperate zone (Shen et al., 2010), and even in northern polar regions (Barker and Knorr, 2007). Millennial-scale climate signals of global scope, including atmospheric CO_2 (Ahn and Brook, 2008) and sea-level changes (Siddall et al., 2003), are also consistent with the shape of AIM events (EPICA Community Members, 2006).

ASM change is driven by both latent and sensible heat. The SH Indian Ocean is one of the major moisture sources of the ASM

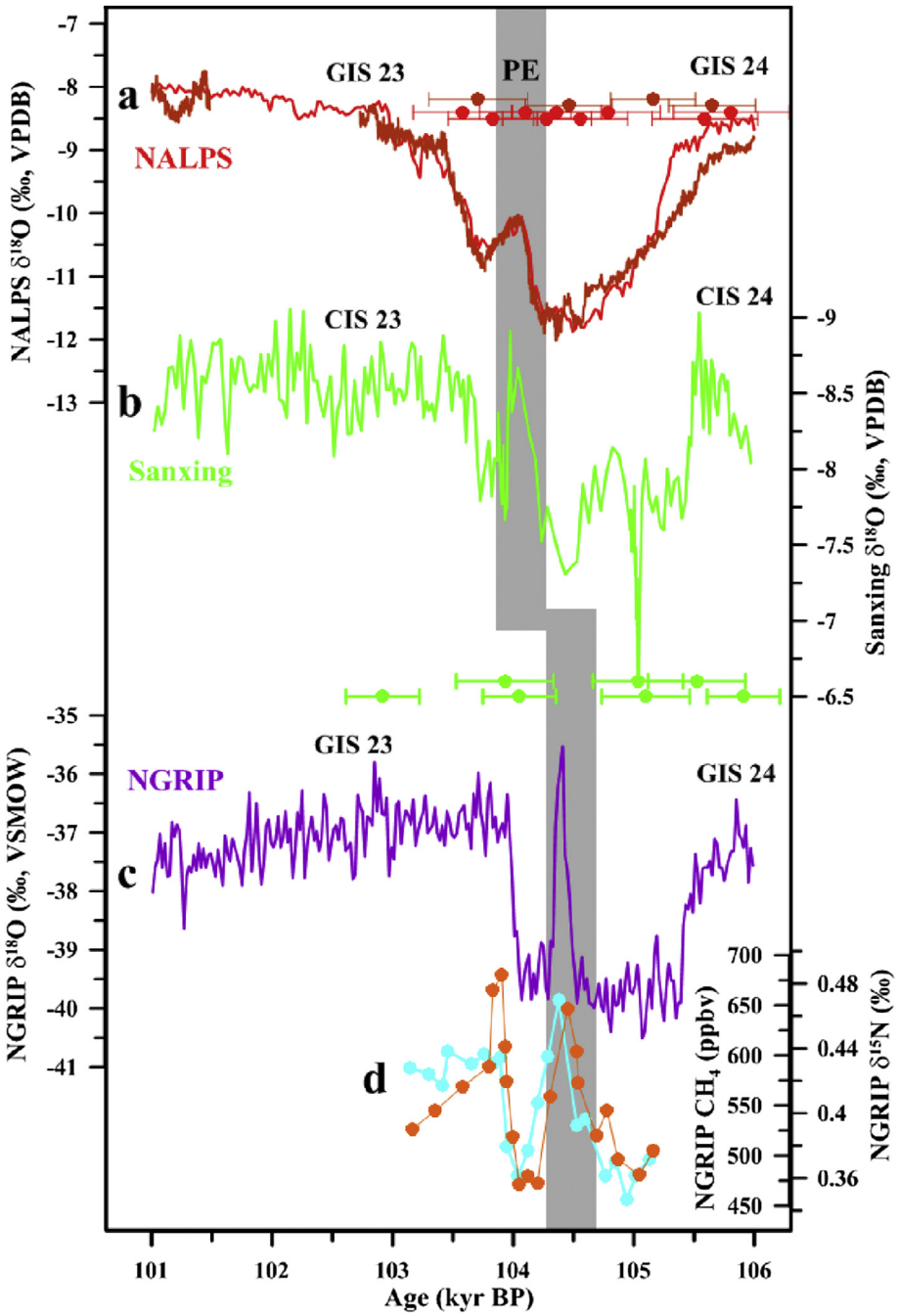

Fig. 6. A short-lived PE preceding GIS 23 registered in **(a)** NALPS $\delta^{18}O$ (red), **(b)** Sanxing $\delta^{18}O$ (green), **(c)** NGRIP $\delta^{18}O$ (purple), and **(d)** NGRIP CH_4 (cyan), and NGRIP $\delta^{15}N$ (orange) data. NGRIP is given on the GICC05modelext timescale (Wolff et al., 2010). GIS 24-23 and CIS 24-23 are the millennial-scale warm/humid events in Greenland and Chinese cave records, respectively. (For interpretation of the references to colour in this figure legend, the reader is referred to the web version of this article.)

(Clemens et al., 1991, 2008; Baker et al., 2015). The strong coupling of the ASM and Antarctic temperature (Fig. 7b, c) suggests a forcing mechanism associated with latent heat distribution, which is determined by the amount of moisture across the equator (Clemens et al., 1991). Previously studies suggested that SH high-latitude cooling led to a high temperature gradient in the SH, which induced a strong transequatorial flow and further contributed to an intensified ASM (Cai et al., 2006; Liu et al., 2008; An et al., 2011; Rohling et al., 2009; Barker and Knorr, 2007). The strong correlation between the Sanxing and the EDML $\delta^{18}O$ records indicates that SH climate may also have regulated the millennial-scale monsoon variability during MIS 5. The AM, as an integral component of the global climate system, may therefore link NH and SH climates via a combined influence of NH pull and SH push (Rohling et al., 2009; An et al., 2011).

5. Conclusions

Using three spliced stalagmites $\delta^{18}O$ time series from Sanxing Cave in southwestern China, we reconstructed a detailed history of the ASM from 113.5 to 86.6 kyr BP. Synchroneity with published records from other Chinese caves demonstrates that the ASM

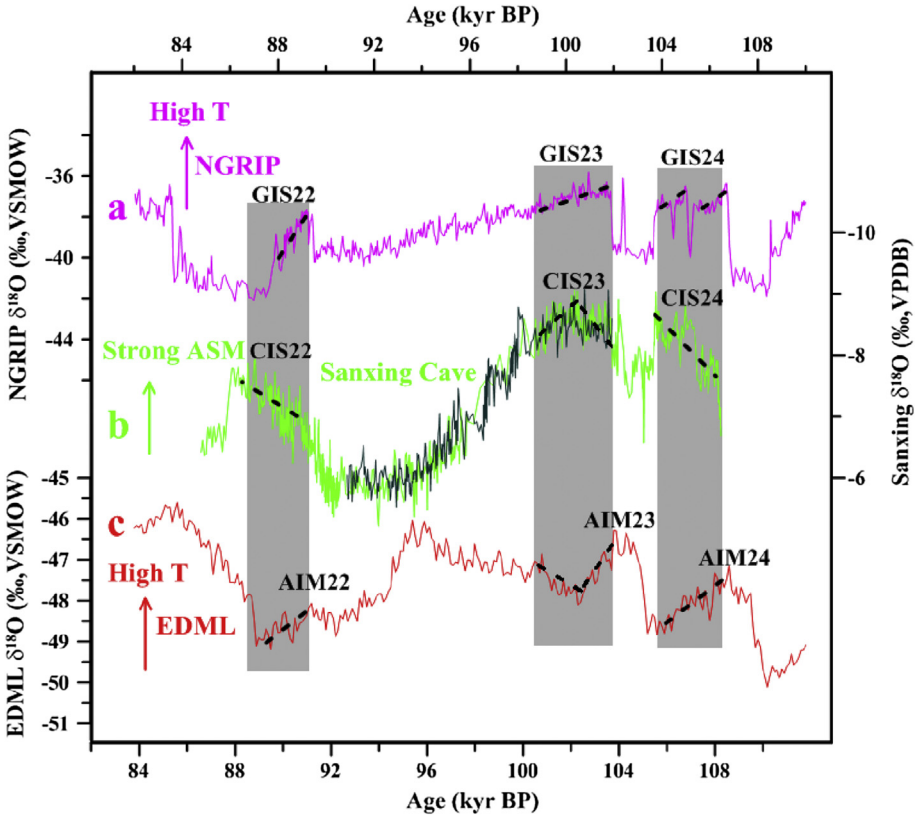

Fig. 7. Comparison of $\delta^{18}O$ records between Sanxing Cave, and Greenland and Antarctica ice cores. **(a)** NGRIP record, **(b)** Sanxing stalagmite record, **(c)** EDML record. The Sanxing age model is based on ^{230}Th dates (lower X axis), while NGRIP and EDML are on the EDML1 timescale (Capron et al., 2010b; upper X axis). GIS 22-24, CIS 22-24, and AIM 22-24 are the millennial-scale warm and humid events in Greenland, China, and Antarctica, respectively. Three gray vertical bars at 90, 102, and 107 kyr BP mark the different climate change trends in Greenland and southwestern China, influenced by thermal dynamics in the SH, expressed in the EDML record.

intensity primarily follows NHSI on orbital timescales. This new cave record also reveals a centennial-scale PE preceding CIS 23. The record also exhibits four strong monsoon events, CIS 25-22, consistent with millennial climatic changes in Greenland, but with an offset of up to 2.3 kyr. The new speleothem chronology with dating uncertainties of only ±0.3–0.6 kyr offers the potential for improving timescales of other proxy records. The anti-phase behavior between the Sanxing record and the EDML ice-core $\delta^{18}O$ record implies a link between ASM and SH temperature.

Acknowledgments

Authors would like to thank K. Lin for her assistance in the laboratory. Reviews by several anonymous reviewers greatly improved this manuscript. This study was supported by the National Natural Science Foundation of China (41372189, U1405231 to X.J. and 41463014 to Y.H.). Funding was also provided by grants from Taiwan ROC MOST (103-2119-M-002-022 and 104-2119-M-002-003 to C.-C.S.) and the National Taiwan University (105R7625 to C.-C.S.).

Appendix A. Supplementary data

Supplementary data related to this article can be found at http://dx.doi.org/10.1016/j.quascirev.2016.05.003.

References

Ahn, J., Brook, E.J., 2008. Atmospheric CO_2 and climate on millennial time scales during the last glacial period. Science 322, 83–85.

Altabet, M.A., Higginson, M.J., Murray, D.W., 2002. The effect of millennial-scale changes in Arabian Sea denitrification on atmospheric CO_2. Nature 415, 159–162.

An, Z., Clemens, S.C., Shen, J., Qiang, X., Jin, Z., Sun, Y., Prell, W.L., Luo, J., Wang, S., Xu, H., Cai, Y., Zhou, W., Liu, X., Liu, W., Shi, Z., Yan, L., Xiao, X., Chang, H., Wu, F., Ai, L., Lu, F., 2011. Glacial-interglacial Indian summer monsoon dynamics. Science 333, 719–723.

Baker, A.J., Sodemann, H., Baldini, J.U.L., Breitenbach, S.F.M., Johnson, K.R., van Hunen, J., Zhang, P., 2015. Seasonality of westerly moisture transport in the East Asian summer monsoon and its implications for interpreting precipitation $\delta^{18}O$. J. Geophys. Res. Atmos. 120 http://dx.doi.org/10.1002/2014JD022919.

Barker, S., Knorr, G., 2007. Antarctic climate signature in the Greenland ice core record. Proc. Natl. Acad. Sci. U.S.A. 104, 17278–17282.

Berger, A., Loutre, M.F., 1991. Insolation values for the climate of the last 10 million years. Quat. Sci. Rev. 10, 297–317.

Blunier, T., Brook, E.J., 2001. Timing of millennial-scale climate change in Antarctica and Greenland during the last glacial period. Science 291, 109–112.

Blunier, T., Chappellaz, J., Schwander, J., Dallenbach, A., Stauffer, B., Stocker, T.F., Raynaud, D., Jouzel, J., Clausen, H.B., Hammer, C.U., Johnsen, S.J., 1998. Asynchrony of Antarctic and Greenland climate change during the last glacial period. Nature 394, 739–743.

Blunier, T., Spahni, R., Barnola, J.M., Chappellaz, J., Loulergue, L., Schwander, J., 2007. Synchronization of ice core records via atmospheric gases. Clim. Past. 3, 325–330.

Boch, R., Cheng, H., Spötl, C., Edwards, R.L., Wang, X., Häuselmann, P., 2011. NALPS: a precisely dated European climate record 120–60 ka. Clim. Past. 7, 1247–1259.

Cai, Y., An, Z., Cheng, H., Edwards, R.L., Kelly, M.J., Liu, W., Wang, X., Shen, C.-C., 2006. High-resolution absolute-dated Indian monsoon record between 53 and 36 ka from Xiaobailong Cave, southwestern China. Geology 34, 621–624.

Capron, E., Landais, A., Chappellaz, J., Schilt, A., Buiron, D., Dahl-Jensen, D., Johnsen, S.J., Jouzel, J., Lemieux-Dudon, B., Loulergue, L., Leuenberger, M., Masson-Delmotte, V., Meyer, H., Oerter, H., Stenni, B., 2010a. Millennial and sub-millennial scale climatic variations recorded in polar ice cores over the last glacial period. Clim. Past. 6, 345–365.

Capron, E., Landais, A., Lemieux-Dudon, B., Schilt, A., Masson-Delmotte, V., Buiron, D., Chappellaz, J., Dahl-Jensen, D., Johnsen, S.J., Leuenberger, M., Loulergue, L., Oerter, H., 2010b. Synchronising EDML and NorthGRIP ice cores using $\delta^{18}O$ of atmospheric oxygen ($\delta^{18}O_{atm}$) and CH_4 measurements over MIS 5 (80–123 kyr). Quat. Sci. Rev. 29, 222–234.

Cheng, H., Edwards, R.L., Broecker, W.S., Denton, G.H., Kong, X., Wang, Y., Zhang, R., Wang, X., 2009. Ice age terminations. Science 326, 248–252.
Cheng, H., Edwards, R.L., Shen, C.-C., Polyak, V.J., Asmerom, Y., Woodhead, J., Hellstrom, J., Wang, Y., Kong, X., Spötl, C., Wang, X., Alexander, E.C., 2013. Improvements in ^{230}Th dating, ^{230}Th and ^{234}U half-life values, and U-Th isotopic measurements by multi-collector inductively coupled plasma mass spectrometry. Earth Planet. Sci. Lett. 372, 82–91.
Cheng, H., Sinha, A., Wang, X., Cruz, F.W., Edwards, R.L., 2012. The global Paleomonsoon as seen through speleothem records from Asia and the Americas. Clim. Dyn. 39, 1045–1062.
Clemens, S., Prell, W., Murray, D., Shimmield, G., Weedon, G., 1991. Forcing mechanisms of the Indian Ocean monsoon. Nature 353, 720–725.
Clemens, S.C., Prell, W.L., Sun, Y.B., Liu, Z.Y., Chen, G.S., 2008. Southern Hemisphere forcing of Pliocene δ^{18}O and the evolution of Indo-Asian monsoons. Paleoceanography 23, PA4210. http://dx.doi.org/10.1029/2008PA001638.
Cruz, F.W., Karmann, I., Viana, O.J., Burns, S.J., Ferrari, J.A., Vuille, M., Sial, A.N., Moreira, M.Z., 2005. Stable isotope study of cave percolation waters in subtropical Brazil: implications for paleoclimate inferences from speleothems. Chem. Geol. 220, 245–262.
Dansgaard, W., Johnsen, S.J., Clausen, H.B., Dahl-Jensen, D., Gunderstrup, N.S., Hammer, C.U., Steffensen, J.P., Sveinbjörnsdottir, A., Jouzel, J., Bond, G., 1993. Evidence for general instability of past climate from a 250-kyr ice-core record. Nature 364, 218–220.
Dayem, K.E., Molnar, P., Battisti, D.S., Roe, G.H., 2010. Lessons learned from oxygen isotopes in modern precipitation applied to interpretation of speleothem records of paleoclimate from eastern Asia. Earth Planet. Sci. Lett. 295, 219–230.
Deplazes, G., Lückge, A., Peterson, L.C., Timmermann, A., Hamann, Y., Hughen, K.A., Röhl, U., Laj, C., Cane, M.A., Sigman, D.M., Haug, G.H., 2013. Links between tropical rainfall and North Atlantic climate during the last glacial period. Nat. Geosci. 6, 213–217.
Deplazes, G., Lückge, A., Stuut, J.B.W., Pätzold, J., Kuhlmann, H., Husson, D., Fant, M., Haug, G.H., 2014. Weakening and strengthening of the Indian monsoon during Heinrich events and Dansgaard-Oeschger oscillations. Paleoceanography 29, 99–114.
Dorale, J.A., Liu, Z., 2009. Limitations of Hendy test criteria in judging the paleoclimate suitability of speleothems and the need for replication. J. Cave Karst Stud. 71, 38–73.
Duan, F., Liu, D., Cheng, H., Wang, X., Wang, Y., Kong, X., Chen, S., 2014. A high resolution monsoon record of millennial-scale oscillations during Late MIS 3 from Wulu Cave, south-west China. J. Quat. Sci. 29, 83–90.
Duan, F., Wu, J., Wang, Y., Edwards, R.L., Cheng, H., Kong, X., Zhang, W., 2015. A 3000-yr annually laminated stalagmite record of the last Glacial Maximum from Hulu Cave. China. Quat. Res. 83, 360–369.
EPICA Community Members, 2006. One to one coupling of glacial climate variability in Greenland and Antarctica. Nature 444, 195–198.
Fleitmann, D., Burns, S.J., Mangini, A., Mudelsee, M., Kramers, J., Villa, I., Neff, U., Al-Subbarye, A.A., Buettnera, A., Hipplera, D., Matter, A., 2007. Holocene ITCZ and Indian monsoon dynamics recorded in stalagmites from Oman and Yemen (Socotra). Quat. Sci. Rev. 26, 170–188.
Genty, D., Blamart, D., Ouahdi, R., Gilmour, M., Baker, A., Jouzel, J., Van-Exter, S., 2003. Precise dating of Dansgaard-Oeschger climate oscillations in western Europe from stalagmite data. Nature 421, 833–837.
Gupta, A.K., Anderson, D.M., Overpeck, J.T., 2003. Abrupt changes in the Asian southwest monsoon during the Holocene and their links to the North Atlantic Ocean. Nature 421, 354–357.
Hendy, C.H., 1971. The isotopic geochemistry of speleothems-I. The calculation of the effects of different modes of formation on the isotopic composition of speleothems and their applicability as palaeoclimatic indicators. Geochim. Cosmochim. Acta 35, 801–824.
Kelly, M.J., Edwards, R.L., Cheng, H., Yuan, D., Zhang, M., An, Z., 2006. High resolution characterization of the AM between 146,000 and 99,000 years B.P. from Dongge Cave, China and global correlation of events surrounding Termination II. Palaeogeogr. Palaeoclimatol. Palaeoecol. 236, 20–38.
Landais, A., Masson-Delmotte, V., Jouzel, J., Raynaud, D., Johnsen, S., Huber, C., Leuenberger, M., Schwander, J., Minster, B., 2006. The glacial inception as recorded in the North-GRIP Greenland ice core: timing, structure and associated abrupt temperature changes. Clim. Dyn. 26, 273–284.
Li, C., Battisti, D.S., Bitz, C.M., 2010. Can North Atlantic sea ice anomalies account for Dansgaard–Oeschger climate signals? J. Clim. 23, 5457–5475.
Li, T., Shen, C.-C., Huang, L.-J., Jiang, X., Yang, X., Mii, H.-S., Lee, S.-Y., Lo, L., 2014. Stalagmite-inferred variability of the Asian summer monsoon during the penultimate glacial-interglacial period. Clim. Past. 10, 1211–1219.
Lisiecki, L.E., Raymo, M.E., 2005. A Pliocene-Pleistocene stack of 57 globally distributed benthic δ^{18}O records. Paleoceanography 20, PA1003. http://dx.doi.org/10.1029/2004PA001071.
Liu, D., Wang, Y., Cheng, H., Edwards, R.L., Kong, X., Wang, X., Wu, J., Chen, S., 2008. A detailed comparison of Asian monsoon intensity and Greenland temperature during the Allerød and Younger Dryas events. Earth Planet. Sci. Lett. 272, 691–697.
Liu, D., Wang, Y., Cheng, H., Edwards, R.L., Kong, X., Wang, X., Hardt, B., Wu, J., Chen, S., Jiang, X., He, Y., Dong, J., Zhao, K., 2010. Sub-millennial variability of Asian monsoon intensity during the early MIS 3 and its analogue to the ice age terminations. Quat. Sci. Rev. 29, 1107–1115.
Liu, J., Chen, J., Zhang, X., Li, Y., Rao, Z., Chen, F., 2015. Holocene East Asian summer monsoon records in northern China and their inconsistency with Chinese stalagmite δ^{18}O records. Earth-Sci. Rev. 148, 194–208.
Liu, Z., Wen, X., Brady, E.C., Otto-Bliesner, B., Yu, G., Lu, H., Cheng, H., Wang, Y., Zheng, W., Ding, Y., Edwards, R.L., Cheng, J., Liu, W., Yang, H., 2014. Chinese cave records and the East Asia summer monsoon. Quat. Sci. Rev. 83, 115–128.
Maher, B.A., 2008. Holocene variability of the East Asian summer monsoon from Chinese cave records: a re-assessment. Holocene 18, 861–866.
McManus, J.F., Oppo, D.W., Cullen, J.L., 1999. A 0.5-million-year record of millennial-scale climate variability in the North Atlantic. Science 283, 971–975.
Meyer, M.C., Cliff, R.A., Spötl, C., Knipping, M., Mangini, A., 2009. Speleothems from the earliest Quaternary: snapshots of paleoclimate and landscape evolution at the northern rim of the Alps. Quat. Sci. Rev. 28, 1374–1391.
Mikolajewicz, U., Crowley, T.J., Schiller, A., Voss, R., 1997. Modelling teleconnections between the North Atlantic and North Pacific during the Younger Dryas. Nature 387, 384–387.
North Greenland Ice Core Project Members, 2004. High-resolution record of Northern Hemisphere climate extending into the last interglacial period. Nature 431, 147–151.
Partin, J.W., Cobb, K.M., Adkins, J.F., Clark, B., Fernandez, D.P., 2007. Millennial-scale trends in west Pacific warm pool hydrology since the Last Glacial Maximum. Nature 449, 452–455.
Pausata, F.S.R., Battisti, D.S., Nisancioglu, K.H., Bitz, C.M., 2011. Chinese stalagmite δ^{18}O controlled by changes in the Indian monsoon during a simulated Heinrich event. Nat. Geosci. 4, 474–480.
Rohling, E.J., Liu, Q.S., Roberts, A.P., Stanford, J.D., Rasmussen, S.O., Langen, P.L., Siddall, M., 2009. Controls on the East Asian monsoon during the last glacial cycle, based on comparison between Hulu Cave and polar ice-core records. Quat. Sci. Rev. 28, 3291–3302.
Rousseau, D.D., Kukla, J., McManus, J., 2006. What is what in the ice and the ocean? Quat. Sci. Rev. 25, 2025–2030.
Ruth, U., Barnola, J.M., Beer, J., Bigler, M., Blunier, T., Castellano, E., Fischer, H., Fundel, F., Huybrechts, P., Huybrechts, P., Kipfstuhl, S., Lambrecht, A., Morganti, A., Oerter, H., Parrenin, F., Rybak, O., Severi, M., Udisti, R., Wilhelms, F., Wolff, E., 2007. "EDML1": a chronology for the EPICA deep ice core from Dronning Maud Land, Antarctica, over the last 150 000 years. Clim. Past. 3, 475–484.
Shackleton, N.J., 1987. Oxygen isotopes, ice volume and sea level. Quat. Sci. Rev. 6, 183–190.
Shen, C.-C., Edwards, R.L., Cheng, H., Dorale, J.A., Thomas, R.B., Moran, S.B., Weinstein, S.E., Edmonds, H.N., 2002. Uranium and thorium isotopic concentration measurements by magnetic sector inductively coupled plasma mass spectrometry. Chem. Geol. 185, 165–178.
Shen, C.-C., Kano, A., Hori, M., Lin, K., Chiu, T.-C., Burr, G.S., 2010. East Asian monsoon evolution and reconciliation of climate records from Japan and Greenland during the last deglaciation. Quat. Sci. Rev. 29, 3327–3335.
Shen, C.-C., Wu, C.-C., Cheng, H., Edwards, R.L., Hsieh, Y.-T., Gallet, S., Chang, C.-C., Li, T., Lam, D.D., Kano, A., Hori, M., Spötl, C., 2012. High-precision and high-resolution carbonate ^{230}Th dating by MC-ICP-MS with SEM protocols. Geochim. Cosmochim. Acta 99, 71–86.
Siddall, M., Rohling, E.J., Almogi-Labin, A., Hemleben, C., Meischner, D., Schmelzer, I., Smeed, D.A., 2003. Sea-level fluctuations during the last glacial cycle. Nature 423, 853–858.
Spötl, C., Mangini, A., Richards, D.A., 2006. Chronology and paleoenvironment of marine isotope stages 3 from two high-elevation speleothems, Austrian Alps. Quat. Sci. Rev. 25, 1127–1136.
Stocker, T.F., Johnsen, S.J., 2003. A minimum thermodynamic model for the bipolar seesaw. Paleoceanography 18, 1087. http://dx.doi.org/10.1029/2003PA000920.
Stott, L., Poulsen, C., Lund, S., Thunell, R., 2002. Super ENSO and global climate oscillations at millennial time scales. Science 297, 222–226.
Sun, Y., Clemens, S.C., Morrill, C., Lin, X., Wang, X., An, Z., 2011. Influence of Atlantic meridional overturning circulation on the East Asian winter monsoon. Nat. Geosci. 5, 46–49.
Svensson, A., Andersen, K.K., Bigler, M., Clausen, H.B., Dahl-Jensen, D., Davies, S.M., Johnsen, S.J., Muscheler, R., Parrenin, F., Rasmussen, S.O., Röthlisberger, R., Seierstad, I., Steffensen, J.P., Vinther, B.M., 2008. A 60 000 year Greenland stratigraphic ice core chronology. Clim. Past. 4, 47–57.
Tan, M., 2014. Circulation effect: response of precipitation δ^{18}O to the ENSO cycle in monsoon regions of China. Clim. Dyn. 42, 1067–1077.
Veres, D., Bazin, L., Landais, A., Toye Mahamadou Kele, H., Lemieux-Dudon, B., Parrenin, F., Martinerie, P., Blayo, E., Blunier, T., Capron, E., Chappellaz, J., Rasmussen, S.O., Severi, M., Svensson, A., Vinther, B., Wolff, E.W., 2013. The Antarctic ice core chronology (AICC2012): an optimized multi-parameter and multi-site dating approach for the last 120 thousand years. Clim. Past. 9, 1733–1748.
Vidal, L., Labeyrie, L., van Weering, T.C.E., 1998. Benthic δ^{18}O records in the North Atlantic over the Last Glacial period (60–10 kyr): evidence for brine formation. Paleoceanography 13, 245–251.
Wang, Y., Cheng, H., Edwards, R.L., An, Z., Wu, J., Shen, C.-C., Dorale, J.A., 2001. A high-resolution absolute-dated late Pleistocene monsoon record from Hulu Cave, China. Science 294, 2345–2348.
Wang, Y., Cheng, H., Edwards, R.L., He, Y., Kong, X., An, Z., Wu, J., Kelly, M.J., Dykoski, C.A., Li, X., 2005. The Holocene Asian monsoon: links to solar changes and North Atlantic climate. Science 308, 854–857.
Wang, Y., Cheng, H., Edwards, R.L., Kong, X., Shao, X., Chen, S., Wu, J., Jiang, X., An, Z., 2008. Millennial-and orbital-scale changes in the East Asian monsoon over the past 224,000 years. Nature 451, 1090–1093.

Wolff, E.W., Chappellaz, J., Blunier, T., Rasmussen, S.O., Svensson, A., 2010. Millennial-scale variability during the last glacial: the ice core record. Quat. Sci. Rev. 29, 2828–2838.
Yancheva, G., Nowaczyk, N.R., Mingram, J., Dulski, P., Schettler, G., Negendank, J.F.W., Liu, J.Q., Sigman, D.M., Peterson, L.C., Haug, G.H., 2007. Influence of the intertropical convergence zone on the East Asian monsoon. Nature 445, 74–77.
Yuan, D., Cheng, H., Edwards, R.L., Dykoski, C.A., Kelly, M.J., Zhang, M., Qing, J., Lin, Y., Wang, Y., Wu, J., Dorale, J.A., An, Z., Cai, Y., 2004. Timing, duration, and transitions of the last interglacial Asian monsoon. Science 304, 575–578.
Zhang, W., Wu, J., Wang, Y., Wang, Y., Cheng, H., Kong, X., Duan, F., 2014. A detailed East Asian monsoon history surrounding the 'Mystery Interval' derived from three Chinese speleothem records. Quat. Res. 82, 154–163.
Zhao, K., Wang, Y., Edwards, R.L., Cheng, H., Liu, D., 2010. High-resolution stalagmite $\delta^{18}O$ records of Asian monsoon changes in central and southern China spanning the MIS 3/2 transition. Earth Planet. Sci. Lett. 298, 191–198.
Zhao, K., Wang, Y., Edwards, R.L., Cheng, H., Liu, D., Kong, X., 2015. A high-resolved record of the Asian summer monsoon from Dongge Cave, China for the past 1200 years. Quat. Sci. Rev. 122, 250–257.
Zhou, H., Zhao, J., Zhang, P., Shen, C.-C., Chi, B., Feng, Y., Lin, Y., Guan, H., You, C.-F., 2008. Decoupling of stalagmite-derived Asian summer monsoon records from North Atlantic temperature change during marine oxygen isotope stage 5d. Quat. Res. 70, 315–321.